Environmental Science & Technology

Article

Cite This: Environ. Sci. Technol. 2018, 52, 5246−5258

pubs.acs.org/est

Simultaneous Improvement of Antimicrobial, Antifouling, and Transport Properties of Forward Osmosis Membranes with Immobilized Highly-Compatible Polyrhodanine Nanoparticles

Ahmad Rahimpour,*[,†] S. Fatemeh Seyedpour,[†] Sadegh Aghapour Aktij,[†] Mostafa Dadashi Firouzjaei,[‡] Alireza Zirehpour,[†] Ahmad Arabi Shamsabadi,[§] Saeed Khoshhal Salestan,[†] Mostafa Jabbari,[∥] and Masoud Soroush*[,§]

[†]Department of Chemical Engineering, Babol Noushirvani University of Technology, Shariati Avenue, Babol, Mazandaran 4714871167, Iran

[‡]Department of Chemical & Biological Engineering, University of Alabama, Tuscaloosa, Alabama 35487, United States

[§]Department of Chemical and Biological Engineering, Drexel University, Philadelphia, Pennsylvania 19104, United States

[∥]Swedish Centre for Resource Recovery, University of Borås, S-50190 Borås, Sweden

Supporting Information

ABSTRACT: This work shows that incorporating highly compatible polyrhodanine nanoparticles (PRh-NPs) into a polyamide (PA) active layer allows for fabricating forward osmosis (FO) thin-film composite (TFC)-PRh membranes that have simultaneously improved antimicrobial, antifouling, and transport properties. To the best of our knowledge, this is the first reported study of its kind to this date. The presence of the PRh-NPs on the surface of the TFC-PRh membranes active layers is evaluated using FT-IR spectroscopy, SEM, and XPS. The microscopic interactions and their impact on the compatibility of the PRh-NPs with the PA chains were studied using molecular dynamics simulations. When tested in forward osmosis, the TFC-PRh-0.01 membrane (with 0.01 wt % PRh) shows significantly improved permeability and selectivity because of the small size and the high compatibility of the PRh-NPs with PA chains. For example, the TFC-PRh-0.01 membrane exhibits a FO water flux of 41 l/(m^2·h), higher than a water flux of 34 l/(m^2·h) for the pristine TFC membrane, when 1.5 molar NaCl was used as draw solution in the active-layer feed-solution mode. Moreover, the reverse solute flux of the TFC-PRh-0.01 membrane decreases to about 115 mmol/(m^2·h) representing a 52% improvement in the reverse solute flux of this membrane in comparison to the pristine TFC membrane. The surfaces of the TFC-PRh membranes were found to be smoother and more hydrophilic than those of the pristine TFC membrane, providing improved antifouling properties confirmed by a flux decline of about 38% for the TFC-PRh-0.01 membranes against a flux decline of about 50% for the pristine TFC membrane when evaluated with a sodium alginate solution. The antimicrobial traits of the TFC-PRh-0.01 membrane evaluated using colony-forming units and fluorescence imaging indicate that the PRh-NPs hinder cell deposition on the TFC-PRh-0.01 membrane surface effectively, limiting biofilm formation.

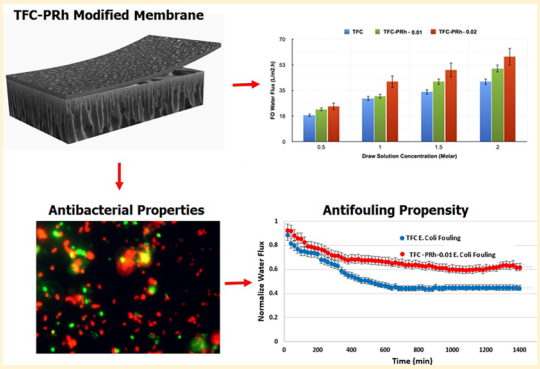

INTRODUCTION

Forward osmosis (FO) is a membranes-based technology that can be used to supply drinking water from seawater and brackish water resources, as well as wastewater reuse. Despite its attractive features, present challenges in developing a FO membrane with a high water permeability, a low reverse solute flux, and negligible fouling propensity have hindered large-scale applications of the FO technology.[1−3] To address these challenges, thin film composite (TFC) polyamide membranes have been developed and used in FO. Although TFC polyamide membranes are known to be less prone to fouling and easy to clean, they undergo organic and biological fouling when used in water treatment, desalination, and wastewater reuse processes.[4−6] As a result of the present unsatisfactory antifouling property of TFC membranes for FO, many studies have been aimed at developing high-performance FO membranes with improved resistance against organic and biological fouling.[1,7]

Another challenge in TFC polyamide membranes is the degradation of the membranes upon exposure to common disinfectants and oxidants such as chlorine or its derivatives,[8] necessitating alternative membrane preparation strategies such as surface coating TFC membranes with hydrophilic functional

Received: February 9, 2018
Accepted: March 28, 2018
Published: March 28, 2018

DOI: 10.1021/acs.est.8b00804
Environ. Sci. Technol. 2018, 52, 5246−5258

Scheme 1. Polymerization Mechanism of Rhodamine[34,35]

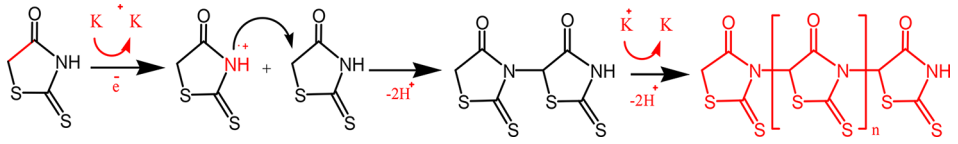

Scheme 2. Postulated Interaction Mechanism of PRh-NPs with the TMC Monomer and PA Chains

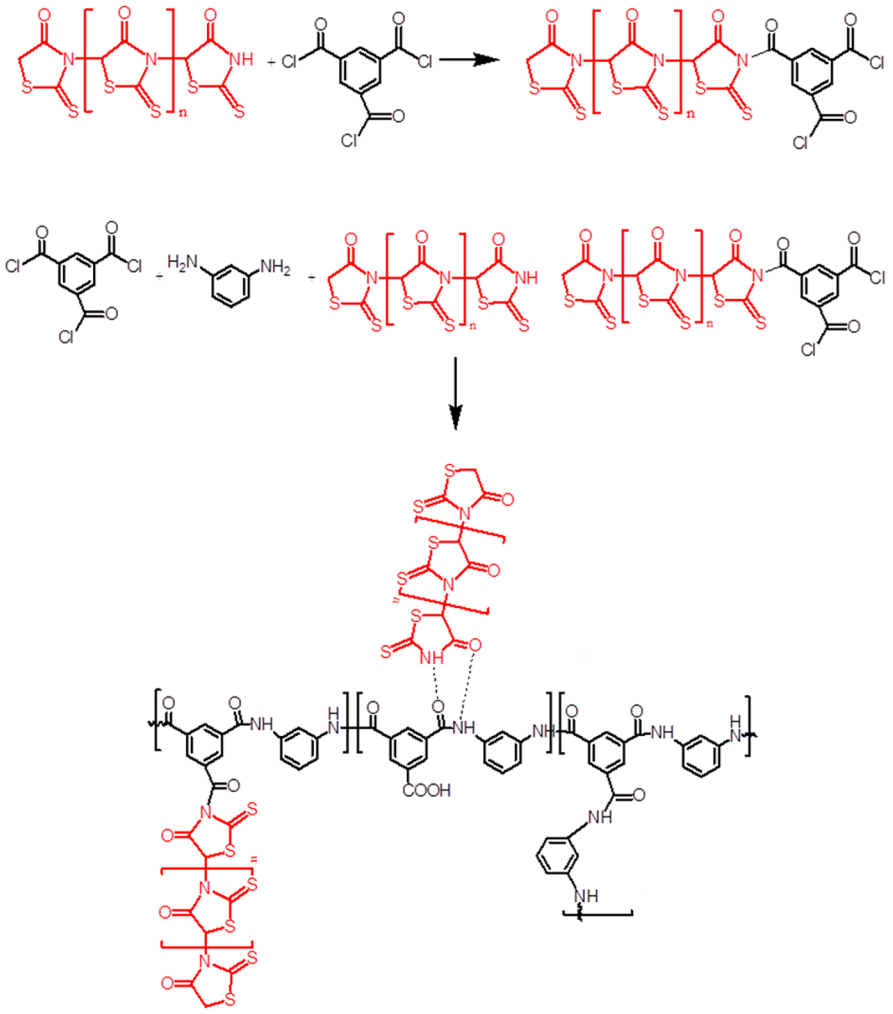

materials and incorporating hydrophilic and antimicrobial materials into the membrane active layer.[9−13] Modifying TFC membranes with superhydrophilic materials increases the membrane resistance to fouling caused by organic molecules such as proteins, polysaccharides, and natural organic matters,[7,9,11] but it compromises the membrane biofouling resistance.[8,12,14] Efforts have been made to incorporate biocidal nanomaterials into TFC membranes as an efficient approach to prevent the attachment or growth of microorganisms on the membrane surface.[15−24] Biocidal nanomaterials such as zinc oxide,[25] silver, and copper nanoparticles,[19,26] have been incorporated into membranes. However, the performance and long-term efficiency of the TFC membranes have been affected negatively by agglomeration and leaching-out of the nanomaterials, caused by the low compatibility of the inorganic materials with polymer chains.[27,28]

Because of their antibacterial, antiviral, and antimicrobial properties, rhodanine and its derivatives have received considerable attention in a wide range of applications.[29−32] Rhodamine-based polymers can be used as antimicrobial agents.[33] In this study, for the first time, highly compatible PRh-NPs are incorporated into the polyamide (PA) active layer of TFC FO membranes to fabricate defect-free thin films with simultaneously improved transport, antifouling, and bactericidal properties. The PRh-NPs are synthesized and then are used in the fabrication of TFC-PRh FO membranes. Because of the high compatibility of the PRh-NPs with the PA chains, which facilitates the formation of an integrated defect-free active layer, the TFC-PRh membranes have superior performance. Interactions between the PRh-NPs and the PA chains strongly affect the structure of the PRh-TFC membranes. As the interactions are impossible to characterize using experimental techniques,[34,35] we use molecular dynamic (MD) simulations to gain insights into them. This Article reports a study that makes a synergetic use of laboratory experiments and MD simulations to

DOI: 10.1021/acs.est.8b00804
Environ. Sci. Technol. 2018, 52, 5246−5258

gain a good understanding of the microscopic interactions and the compatibility of PRh-NPs with PA chains.

MATERIAL AND METHODS

Materials and Chemicals. *N*,*N*-Dimethylformamide (DMF, 99.5%,), Triton X-100, polyvinylpyrrolidone (PVP, M_w = 25000 g/mol), trimesoyl chloride (TMC), 1,3-phenylendiamine (MPD), triethylamine (TEA), camphorsulfonic acid (CSA), *n*-hexane (96%, Scharlau), sodium chloride (NaCl, 99.5%), rhodanine monomer (2-thioxo-4-thiazolidinone), dodecylbenzenesulfonate (DBSNa), and potassium permanganate ($KMnO_4$) were purchased from Merck. Poly(ether sulfone) (PES) (Ultrason E6020P, M_W = 58 000 g/mol) was purchased from BASF. *Escherichia (E.) coli* (ATCC 25922) and *Staphylococcus (S.)* (ATCC 25923) were provided by Razi Vaccine and Serum Research Institute (Karaj, Iran).

PRh-NPs Synthesis and Characterization. 1.13 μmoles of rhodanine (monomer) was dissolved in 50 mL of deionized water, and the solution was heated up to 70 °C. A DBSNa solution (0.86 μmol of DBSNa in 30 mL of water) was added to the rhodamine solution under stirring. The temperature of the resulting solution was then decreased gradually to 40 °C. After 30 min, 50 mL of 63.2 mmol/L $KMnO_4$ solution was added slowly dropwise to the rhodamine-DBSNa solution. The oxidation polymerization of rhodanine was completed after 20 h at 25 °C. The solution was then centrifuged and washed three times with acetone and deionized water to obtain PRh-NPs. The resulting residue was dried under vacuum at 45 °C for 2 days. The polymerization mechanism of rhodamine monomer is shown in Scheme 1.

The PRh-NPs were characterized using transmission electron microscopy (TEM), scanning electron microscopy (SEM), and Fourier transform infrared (FT-IR) spectroscopy. A MasterSizer laser diffraction particle size analyzer was used to determine the particle size distribution of the PRh-NPs. The size of the PRh particles in the DMF solvent was measured using the dynamic light scattering (DLS) method.

Preparation and Characterization of TFC and TFC-PRh Membranes. Interfacial polymerization (IP) on the surface of PES substrates was carried out to prepare TFC membranes. To prepare the TFC membranes, the PES support was first immersed in a solution containing 2.0 wt % MPD, 1 wt % TEA, and 2 wt % CSA for 2 min. The MPD saturated membranes were dipped in a 0.1 wt./v% TMC in *n*-hexane solution for 30 s (referred to as pristine TFC membranes without the PRh-NPs). The TFC-PRh membranes were fabricated using the same procedure but by incorporating PRh-NPs into the PA layer during IP. Two different levels of the PRh-NPs (0.01 and 0.02 wt %) were loaded in the TMC solution followed by ultrasonicating for 10 min. After the formation of the selective layer, the membranes were cured in an oven at 80 °C for 5 min and stored in 20 °C deionized water before testing. These membranes will be referred to as TFC-PRh-0.01 (with 0.01% PRh-NPs) and TFC-PRh-0.02 (with 0.02% PRh-NPs) membranes. We propose the polymerization mechanism and the interactions among TMC, PA chains, and PRh, shown in Scheme 2. When PRh-NPs are added to the TMC solution, they react with TMC molecules during ultrasonication, and this reaction allows for incorporating PRh-NPs into the PA structure during IP. In addition to the covalent bonds formed by the reaction, the carbonyl and secondary amine groups of the unreacted PRhs interact with the carbonyl and amide groups of the PA backbone via hydrogen bonds.[36] The characterization methods are described in SI.S2.1.

Molecular Dynamic (MD) Simulations. All MD simulations were performed using Materials Studio 6.0 (MS) software (Accelrys Inc., San Diego).[37] Details on the simulation procedure used for the polyrhodanine monomer, polyamide chains, and the PRh-NPs incorporated into the polyamide are provided in SI.S2.2.

Evaluation of Transport Properties and FO Performance. A common lab-scale FO setup with a membrane cell with an effective area of 30 cm^2 was used to measure the FO water and reverse solute fluxes for the pristine TFC and TFC-PRh membranes. More information on the setup and procedure used to measure the FO performance of the membranes are provided in SI.S2.3.

The intrinsic characteristics of the membranes (water permeability, solute permeability, and structural parameter, denoted by A, B, and S, respectively) were evaluated using the protocol described in ref 38. An average value of three independent measurements (from three separate experiments) was used in the calculation of the membrane characteristics.

Antimicrobial Activity Assessment of the Membranes. Two model bacteria, *E. coli* and *S. aureus*, were grown overnight in a Luria−Bertani (LB) broth while shaking the broth at 37 °C. The broth with the grown bacteria was then diluted with a fresh LB broth and was kept under incubation conditions for 3 h. The number of attached live bacteria on the membrane surface was quantified via a viable-cell-attachment experiment (more details on sample preparation for colony counting and fluorescence imaging are provided in SI.S2.4).[39] A Leica DMRXE fluorescence microscope (100× PlanApo objective lens coupled to a digital image capture system, Tucsen model TC-3) was used to record images by the TS View (On Focus Laboratories, version 7) software.

FO Membrane Fouling and Biofouling Assessment Pathway. Dynamic fouling experiments were carried out to evaluate the resistance of TFC and TFC-PRh membranes against organic- and biofouling, according to the procedure described in ref.[40] For the organic fouling assessment, sodium alginate, a polysaccharide, was selected as a model organic foulant (further explanation can be found in SI.S2.5).[40,41]

RESULTS AND DISCUSSION

The PRh-NPs were characterized using SEM, TEM, DLS, and FTIR-ATR. The characterization results and explanations are provided in SI.S3.1.

Microscopic Interaction of PRh-NPs with PA Chain. To gain a better understanding of intermolecular interactions between the PRh-NPs and the PA chains, MD simulations were carried out. The strength of microscopic interactions can be quantified using the interaction energy, $E_{\text{intteraction}}$

$$E_{\text{interaction}} = E_{\text{mixture}} - (E_{\text{polyamide}} + E_{\text{polyrhodanine}}) \quad (1)$$

where E_{mixture} is the total potential energy of the PRh-NPs and PA mixture, $E_{\text{polyamide}}$ is the potential energy of the PA chains, and $E_{\text{Polyrhodanine}}$ is the potential energy of PRh-NPs. The interaction energy can be used to quantify the strength of covalent or H-bond interactions. The calculated interaction energies are given in Table 1. A molecular structure with a negative interaction energy is stable; the more negative is the energy, the more stable is the structure. As can be seen in Table 1, the negative interaction energies confirm proper compatibility and good intermolecular interactions between PRh-NPs and PA chains. However, the interaction energy of PRh-PA is −306.26 kcal/mol,

DOI: 10.1021/acs.est.8b00804
Environ. Sci. Technol. 2018, 52, 5246−5258

Table 1. Energies Calculated Using MD Simulations (kcal/mol)

		$E_{Mixture}$	$E_{polyamide}$	$E_{polyrhodanine}$	$E_{intraction}$
PA−PRh	total energy	320.762	644.122	−17.100	−306.260
	H-bond	−78.019	−55.352	0.000	−22.667
bonded−PA−PRh	total energy	340.242	579.350	−39.820	−199.290
	H-bond	−41.666	−30.145	−3.266	−8.255

which is approximately 53% higher than that of bonded-PRh-PA (−199.29 kcal/mol). The less negative interaction energy of the bonded-PRh-PA can be due to the configuration of the PRh-NPs, which leads to steric hindrance. However, the more negative interaction energy of the PRh-PA is due to the uniform alignment of the PRh-NPs along the PA chains.

A higher interaction between PRh-NPs and the functional groups of PA can be indicative of the formation of hydrogen bonds. In other words, there is a good affinity between oxygen/nitrogen of the PA and the functional groups of the PRh-NPs, which leads to the formation of hydrogen bonds, as schematically shown in Figure 1. Nevertheless, the total interaction energies calculated based on the Dreiding force fields show that the ratio of hydrogen bonds to the total interactions declined from 7.4% to 4.14% by the addition of PRh-NPs to the polyamide chains. This reduction can be due to the steric hindrance of PRh-NPs that imposes additional limitations on the formation of hydrogen bonds in the bonded-PRh-PA compare to that in PRh-PA, in which PRh-NPs are randomly distributed in the PA matrix.

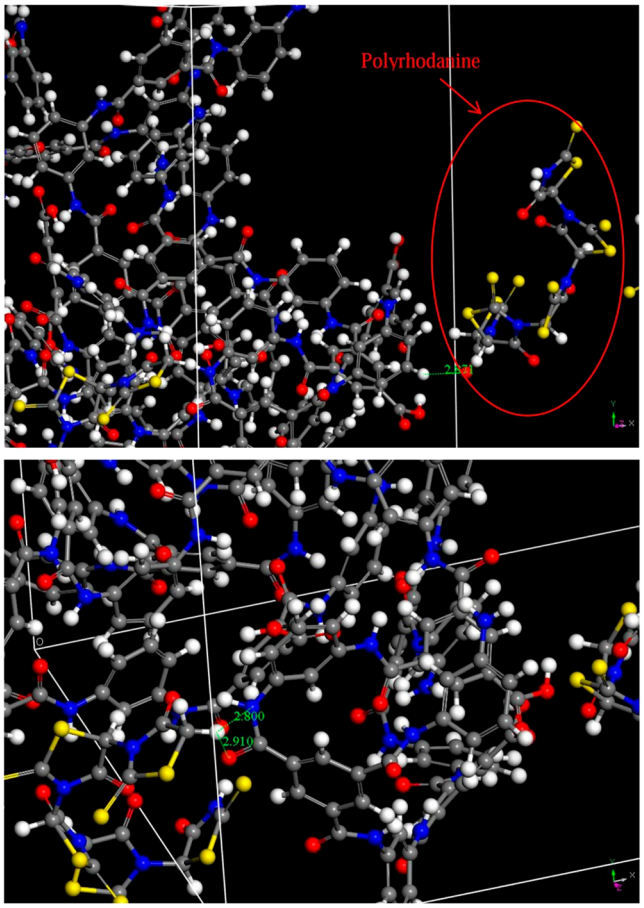

Figure 1. Radial distances between (a) hydrogen and oxygen and (b) hydrogen and nitrogen atoms, where the red, gray, yellow, blue, and white spheres are oxygen, carbon, sulfur, nitrogen, and hydrogen atoms, respectively.

Radial distances between (a) hydrogen and nitrogen atoms and (b) hydrogen and oxygen atoms can also be used to indicate the presence and strength of hydrogen bonds. The H-bond formation probability in a structure has been reported to be maximum at a hydrogen-acceptor distance of 2.7−2.8 Å.[42] As depicted in Figure 1, the calculated distances between the PRh-NPs and the PA chains in both systems is within 2.7−2.9 Å, indicating that the interactions are of the moderate type (electrostatic) based on Jeffrey's categorization.[43]

Surface Characteristics of the Membranes. ATR-FTIR spectroscopy was conducted to analyze the surface chemistry of the TFC and TFC-PRh membranes and the results are presented in Figure 2a. The band at around 1485 cm^{-1} corresponds to the C−C stretching vibrations in the aromatic ring.[41,44] Additionally, the peaks observed at 1145 and 1245 cm^{-1} correspond to the phenyl ring and asymmetric C−O−C stretching vibration related to the PES substrate. The characteristic peaks of the PA layer can be observed in all spectra at 1660 cm^{-1} (amide I, C═O stretching vibration), 1540 cm^{-1} (coupling of C−N and in-plane N−H bending stretching vibration of the amide II), and 1610 cm^{-1} (hydrogen−bonded carbonyl of the amide). As the concentration of the PRh-NPs increased, the intensity of main peaks decreased or disappeared completely,[45] indicating the formation covalent bonds between the PRh-NPs and the PA chains. Interestingly, the intensity of the acyl chloride (550−730 cm^{-1})[46] of the PA layer decreased by increasing the concentration of PRh-NPs, suggesting that new bonds were formed between the PRh-NPs and the unreacted acyl chloride of the PA chains. Moreover, the peak at about 1028 cm^{-1} decreased considerably, and a new peak appeared at 1070 cm^{-1} that can be attributed to the C═S stretching vibration (shifted from 1116 cm^{-1}), verifying the presence of the PRh-NPs in the PA selective layer of the TFC-PRh membranes. The new peak observed at 1442 (shifted from 1431 cm^{-1}) can be assigned to the $C{=}N^{+}$ stretching vibrations of the PRh chains.[47,48] Besides, the considerable decrease of the C═O stretching vibration of the amide I arising from the hydrogen bond formed between the PRh-NPs and the PA chains.[46] Likewise, the gradual increase of the peak intensity at 1544 cm^{-1} with the PRh-NPs concentration suggests the formation of a new amide bond (C−N) between the PRh-NPs and the free acyl chloride of the PA chains.[49]

Increasing the membrane surface hydrophilicity has been found to be an effective strategy to decrease foulant deposition and adhesion on a membrane surface, thereby improving antifouling properties.[50] As can be seen in Figure 2b, incorporating 0.01 and 0.02 wt % of PRh-NPs into the selective layer decreased the contact angle of the TFC membrane from 59° ± 3 to 42° ± 2 and 33° ± 3, respectively; a more hydrophilic surface with higher affinity to water was obtained by embedding PRh-NPs in the PA active layer. The significant improvement in the hydrophilicity of TFC-PRh membranes can be ascribed to the presence of hydrophilic oxygen-containing and amide functional groups in the PRh structure.

An Atomic force microscopy (AFM) analysis was performed to investigate the effects of the PRh on the surface morphology and roughness of the TFC-PRh membranes (Figure 2c). Roughness parameters, average roughness (R_a) and root-mean-squared roughness (R_q), calculated from the AFM images are given in Figure 2d. The AFM images indicate that the TFC-PRh membranes have a much smoother surface compared to the TFC

DOI: 10.1021/acs.est.8b00804
Environ. Sci. Technol. 2018, 52, 5246−5258

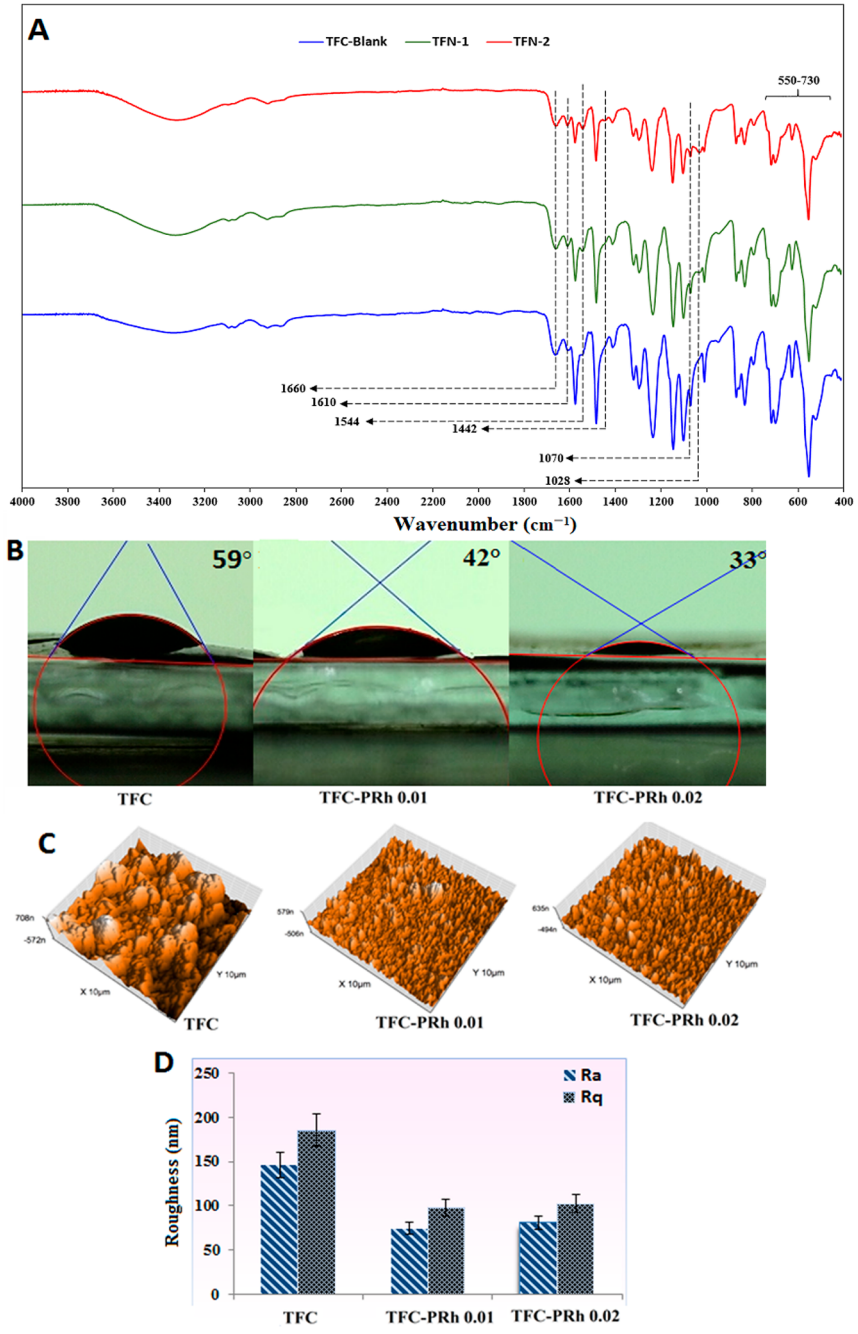

Figure 2. (A) ATR-FTIR spectra, (B) surface contact angles, (C) AFM images, and (D) surface roughness of the TFC and TFC-PRh membranes.

membrane. The PRh-TFC membranes have lower average roughness than the TFC membranes (75 and 81 nm for TFC-PRh-0.02 and TFC-PRh-0.01 membranes, respectively, vs 146 nm for the TFC membranes). This can be attributed to effective dispersion of the PRh-NPs in the active layer and the high compatibility of the PRh-NPs with the PA chains.[51] Also, the average roughness of the TFC-PRh membranes did not change considerably, and there was no statistically significant difference in AFM surface roughness measurements for membranes TFC-PRh-0.01 and TFC-PRh-0.02.

FE-SEM images of the TFC and TFC-PRh membrane surfaces are shown in Figure 3. A homogeneous and typical ridge and valley structure was observed for all TFC membranes, indicating that incorporating the PRh-NPs did not alter the overall structure of the TFC membrane surface considerably. The high-magnification FESEM images show that the presence of PRh-NPs smaller than 50 nm within the active layer and on the surface of both TFC-PRh membranes. Also, the PRh-NPs were well dispersed in the polymer matrix with no considerable agglomeration unlike many other inorganic nanoparticles studied before.[52−54] In addition, it can be seen that the PRh-NPs are surrounded completely by polyamide chains (yellow arrows). This good dispersion of the nanoparticles in the PA structure during IP is a result of the organic and hydrophilic nature of the PRh-NPs. The good compatibility of the PRh-NPs and PA matrix prevents the formation of any interfacial gaps.[40] Figure 4 shows the effect of PRh-NPs loading on the cross-sectional morphology of the TFC membrane active layer. As can be seen, the overall thickness of the active layer decreased slightly with PRh-NPs loading. This decrease in the selective layer

DOI: 10.1021/acs.est.8b00804
Environ. Sci. Technol. 2018, 52, 5246−5258

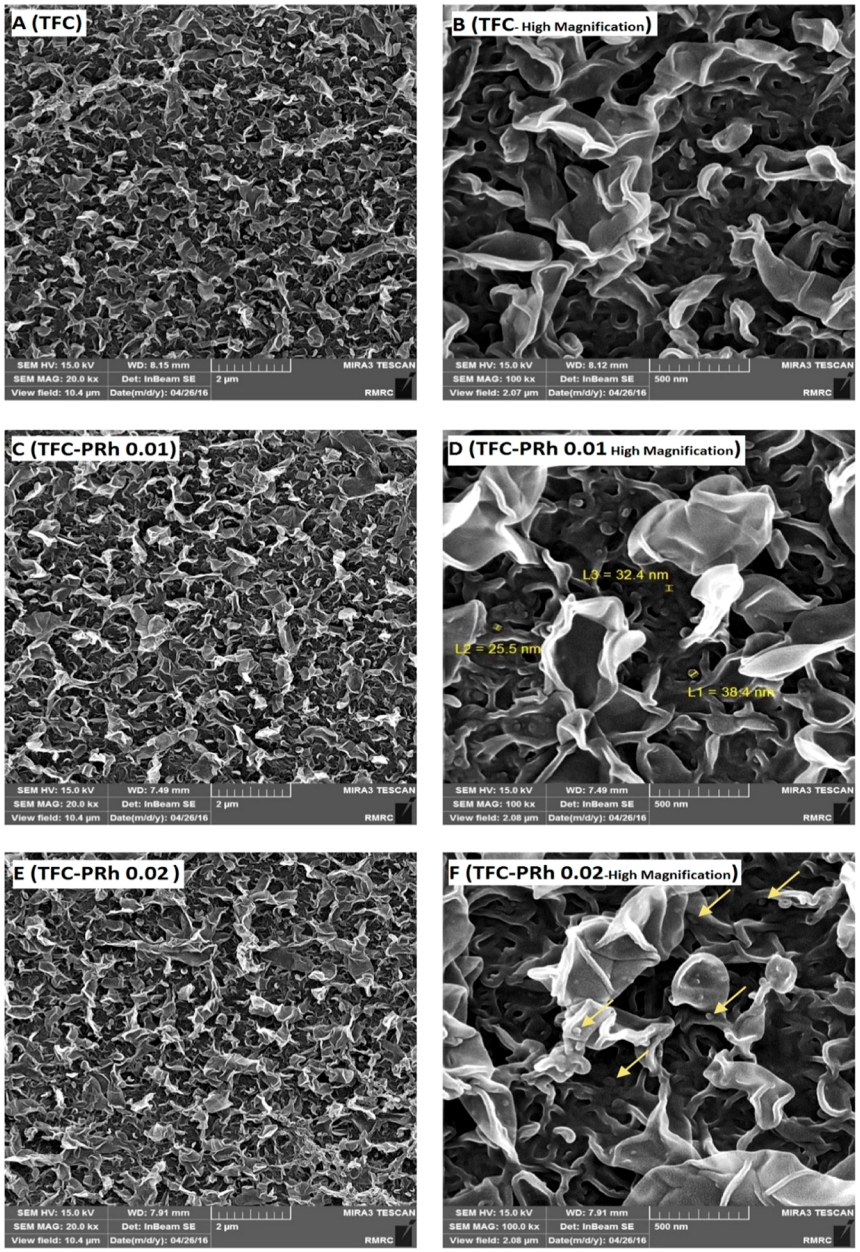

Figure 3. (A, B) Surface FE-SEM images of the TFC membrane, (C, D) TFC-PRh-0.01 membrane, and (E, F) TFC-PRh-0.02 membrane. The right-hand images are high resolution images to better show the PRh-NPs embedded into the active layer.

thickness is due to accelerated the IP caused by loading the hydrophilic PRh-NPs.[55,56] Moreover, the steric hindrance and high compatibility of the PRh-NPs with the amine monomer decrease the MPD penetration and slow the formation of PA, leading to the development of a thinner active layer.[57] Such a reduction in the active layer thickness can lower the mass transfer resistance, leading to an enhanced water flux. However, incorporating a higher concentration of the PRh-NPs increases the likelihood of nanoparticles agglomeration[58−60] and poor dispersion, resulting in the formation of more zigzag channels for water transport and thus lower permeability.

An X-ray photoelectron spectroscopy (XPS) analysis was carried out to investigate the elemental composition, chemical bonding, and degree of cross-linking of the PA selective layer. Figures 5a shows XPS survey spectra of the TFC and TFC-PRh membranes, which point to the presence of three predominant elements, namely oxygen (O 1s), nitrogen (N 1s), and carbon (C 1s). The absence of a sulfur peak in the pristine TFC membrane (the main peak of the support layer) indicates the formation of an integrally skinned PA layer on the surface of the PES support. However, the observation of relatively small signal S (2p) at about 165 eV in the XPS spectra of the TFC-PRh membranes confirms the presence of the PRh-NPs on the surface of these membranes.

Table 2 presents the results of the XPS analysis of the pristine TFC and TFC-PRh membranes, determined based on the intensity of the O (1s), N (1s), C (1s) peaks located at around 532, 399, and 285 eV, respectively.[61] Theoretically, the O/N ratio varies between 1.0, for fully cross-linked structure where each oxygen atom is linked to a nitrogen atom in an amide bond, and 2.0, for a fully linear structure with additional oxygen atoms in the free carboxylic groups.[62] A higher cross-linking degree

DOI: 10.1021/acs.est.8b00804
Environ. Sci. Technol. 2018, 52, 5246−5258

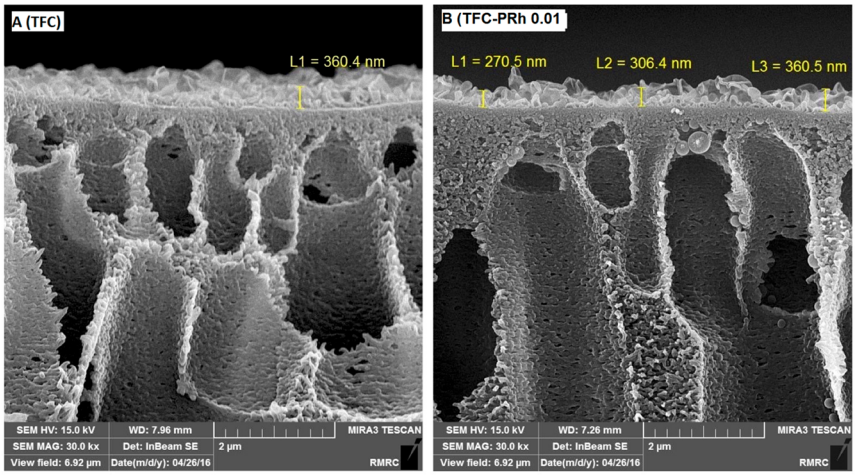

Figure 4. Cross-section FE-SEM images of (A) the TFC membrane and (B) the TFC-PRh-0.01 membrane.

provides a denser polyamide structure and thus higher selectivity, while the carboxylic acid terminal in the linear part is likely responsible for creating improved hydrophilicity and permeability of the surface. The results of the elemental composition analysis indicated that incorporating the PRh-NPs into the TMC solution increases the O/N ratio of the TFC-PRh-0.01 membrane slightly, but that of the TFC-PRh-0.02 membrane considerably. This can be attributed to the presence of oxygen and nitrogen in the structure of the PRh-NPs. The increased O/N ratio can be indicative of a less cross-linked polyamide structure originated from the steric hindrance of the PRh-NPs. The cross-linking degree of a typical PA layer formed by the reaction of MPD and TMC can be determined using the O/N ratio. However, the O/N ratio cannot be representative of the cross-linking degree in the TFC-PRh membranes because of abundant O and N atoms in the structure of PRh-NPs. Consequently, we used the chemical bonds ratio[63] to calculate the cross-linking degree of TFC-PRh membranes. The ratio of chemical bonds was obtained from the deconvolution of the high resolution C 1s and O 1s spectra (Figure 5 and Table 2).[63] Although a lower C═O/C−N ratio can be indicative of a higher content of amide linkage in TFC-PRh membranes,[63] it is not possible to determine the exact O/N or C═O/C−N ratios without considering chemical bonds between the PRh-NPs and the PA chains. The results of both approaches revealed that some of the acyl chloride groups are most presumably consumed by the formation of new bonds between TMC and PRh-NPs, and consequently are incorporated into the polyamide structure during the interfacial polymerization. As can be seen from Figure 5c and 5d, the intensity of the C−N band increased in the TFC-PRh membranes compared to that of TFC ones; this finding agrees with the MD simulations and FTIR spectroscopy results. Both the steric hindrance of the PRh-NPs and the participation of the nanoparticles in the interfacial polymerization weaken the intermolecular bonds between monomer units and decrease the PA layer integrity.[64]

More evidence on the chemical bonding was obtained by deconvolution of C (1s) and O (1s) high-resolution XPS spectra, as shown in Figures 5b and 5c. C (1s) high resolution spectra for both TFC and TFC-PRh membranes show three peaks: a major peak at 285 eV assigned to a carbon atom without adjacent electron withdrawing groups (carbons in aliphatic/aromatic C−C or C−H bonds),[64−66] an intermediate peak at 286.5 eV associated with carbon atoms in a weak electron-withdrawing environment (carbons in C−N bond), and a minor peak at 288.5 eV corresponding to carbons attached to strong electron withdrawing groups (carbons in carboxylic O═C−O and amides O═C−N bonds).[67] High resolution O (1s) spectra of both TFC and TFC-PRh membranes show two peaks at about 531.6 and 533.0 eV (Figures 5d and 5e), which can be assigned to O═C and O−C groups in the PA layer, respectively[48,68] Also, there is an additional peak at 534 eV that corresponds to an O−H bond.[69] As shown in Figure 5f, the high resolution S (2p) spectra of both TFC-PRh-0.01 and TFC-PRh-0.02 membranes has a peak around 165.8 eV, which can be assigned to active S species with a C−S bond.[70] In addition, the peak at 168.3 eV can be attributed to the O−S bond arising from the sulfate species formed by oxidation of S in the air.[71,72]

Transport Properties and Performance Evaluation of Membranes. Table 3 summarizes water permeability (A), solute permeability (B), and structural parameter (S) data for the TFC and TFC-PRh membranes, calculated by the four-step FO measurement method described in ref 24. Generally, incorporating PRh-NPs into the active layer of a TFC membrane leads to improved water permeability. Table 3 shows that 0.01 wt % loading of PRh-NPs into the active layer increased the water permeability, but loading beyond this level decreased the permeability slightly to a value above that of the pristine membrane. However, 0.01 wt % loading of PRh-NPs into the active layer decreased the solute permeability, but loading beyond this level increased the solute permeability to a value much higher that of the pristine membrane. The B value slightly decreased from 0.37 L m^{-2} h^{-1} for the TFC membrane to 0.22 L m^{-2} h^{-1} for the TFC-PRh-0.01 membrane, but increased to 0.55 L m^{-2} h^{-1} for the TFC-PRh-0.02 membrane. An important measure of the selectivity of a FO membrane is the ratio of solute permeability to water permeability, the B/A ratio. A small value of the B/A ratio is desired in FO.[57,70] The B/A ratio of the TFC-PRh-0.01 membrane (0.14 bar^{-1}) is significantly less than that of the TFC and TFC-PRh-0.02 membranes (Table 3). The TFC-PRh-0.02 membrane has the highest B/A ratio compared the other two membranes. Moreover, the salt rejection of TFC-PRh-0.01 membrane was considerably higher than those of the neat TFC and TFC-PRh-0.01 membranes. From these initial performance results, it can be concluded that the low loading rate of PRh-NPs is needed to improve the transport properties of TFC membranes. Incorporating PRh-NPs can influence interfacial polymerization (Scheme 2), resulting in a disrupted

DOI: 10.1021/acs.est.8b00804
Environ. Sci. Technol. 2018, 52, 5246−5258

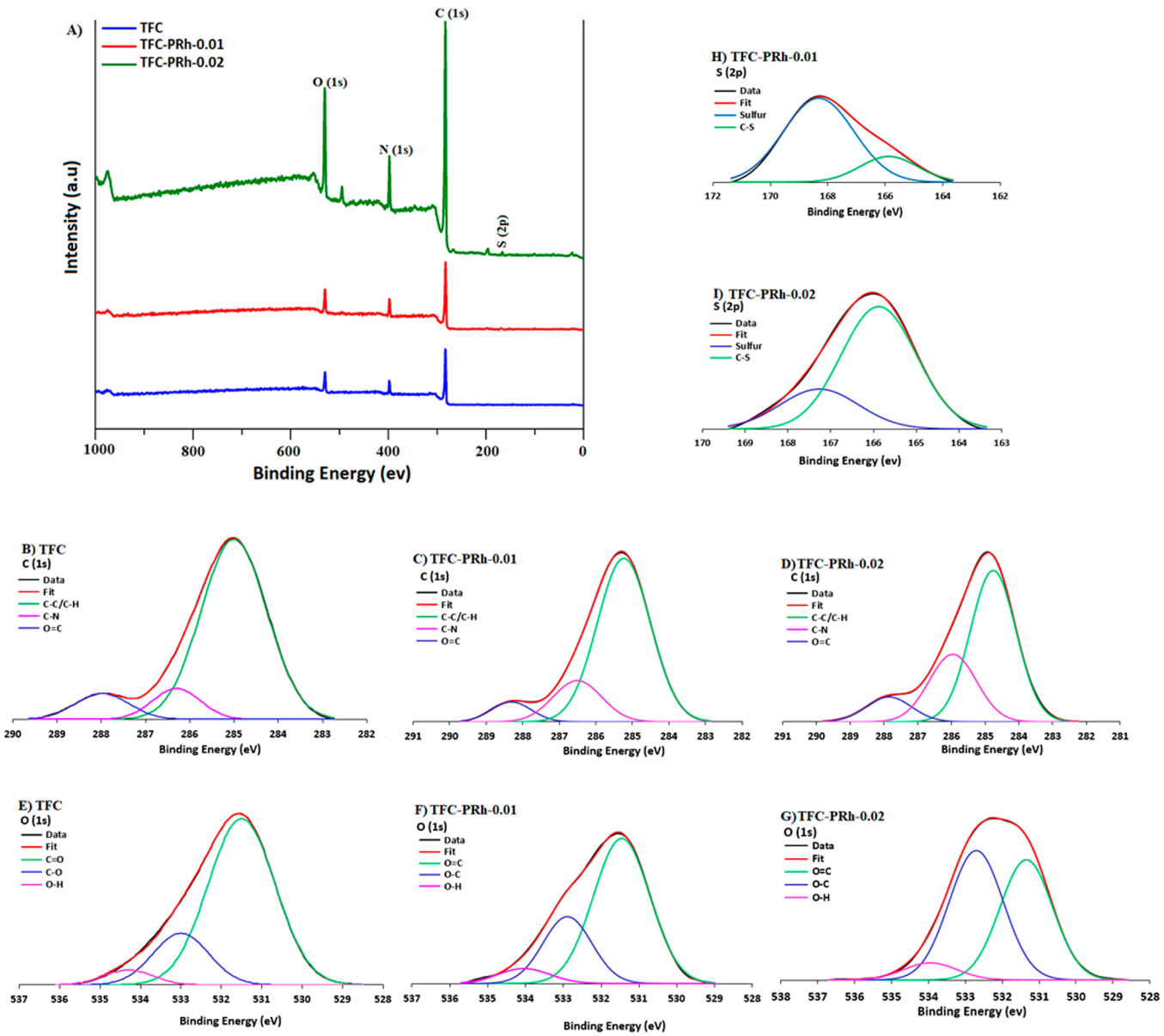

Figure 5. (A) XPS survey spectrum of the TFC membrane and the TFC-PRh-0.01 membrane. Deconvoluted high-resolution C (1s) spectra of (B) TFC membrane, (C) TFC-PRh-0.01 membrane, and (D) TFC-PRh-0.02 membrane. Deconvoluted high-resolution O (1s) spectra of (E) TFC membrane, (F) TFC-PRh-0.01 membrane, and (G) TFC-PRh-0.02 membrane. (H) Deconvoluted high resolution S (2p) spectrum of the TFC-PRh-0.01 membrane, and (I) TFC-PRh-0.02 membrane.

Table 2. Elemental Compositions, O/N Ratio, and Cross-linking Degree of the PA Selective Layer

	atomic concentration (%)						
membrane	C (1s)	O (1s)	N (1s)	S (2p)	O/N ratio	cross-linking degree (%)	C═O/C−N (%)
TFC	81.11	9.29	9.60	0.00	1.03	95.56	37.50
TFC-PRh-0.01	76.20	12.20	11.300	0.37	1.14	80.37	36.23
TFC-PRh-0.01	74.50	14.70	9.30	1.50	1.58	32.56	35.08

polyamide chain packing (see Table 2 for cross-linking degree).[71] The polyamide introduced with lower active layer thickness and less compact structure improves the permeability of TFC-PRh membranes. However, a high loading level of PRh affects the active layer integrity negatively, and hence reduces the selectivity of the membrane. The formation of defects at high concentrations of PRh-NPs can be attributed to the nano-particles agglomeration, poor dispersion, or steric hindrance of bonded-PRh-PA chains. Bonding of PRh-NPs with TMC molecules decreases the degree of cross-linking, deteriorating the PA chains packing, and thus, leading to increased free volume in the selective layer.[59,73,74] However, in case of TFC-PRh-0.01 the presence of abundant intermolecular hydrogen bonds (as proved by the MD simulations) resulted in higher water flux

DOI: 10.1021/acs.est.8b00804
Environ. Sci. Technol. 2018, 52, 5246−5258

Table 3. Intrinsic Transport Properties of the Membranes[a]

membrane	A (L/m^2·h·bar)	B (L/m^2·h)	B/A (bar^{-1})	R (%)	S (μm)
TFC	1.1 ± 0.09	0.37 ± 0.02	0.34 ± 0.045	74.97 ± 2.06	123 ± 1.00
TFC-PRh-0.01	1.6 ± 0.10	0.22 ± 0.01	0.14 ± 0.014	94.65 ± 2.44	128 ± 2.00
TFC-PRh-0.02	1.3 ± 0.10	0.55 ± 0.03	0.42 ± 0.055	60.00 ± 1.78	71 ± 4.00

[a]A = water permeability, B = solute permeability, and S = structural parameter. The salt rejection, R (%), were obtained by experiments with 20 mM NaCl, at 7.5 bar, and at 23 cm/s.

without scarifying the salt selectivity, compared to that of the TFC membrane. Additionally, the more hydrophilic surface of the TFC-PRh membranes can adsorb water molecules more easily, facilitating the transport of water molecules through the active layer.

The water flux (J_w) and solute flux (J_s) of the TFC and TFC-PRh membranes measured at different concentrations of draw solution (DS) are presented in Figures 6a and b. The results

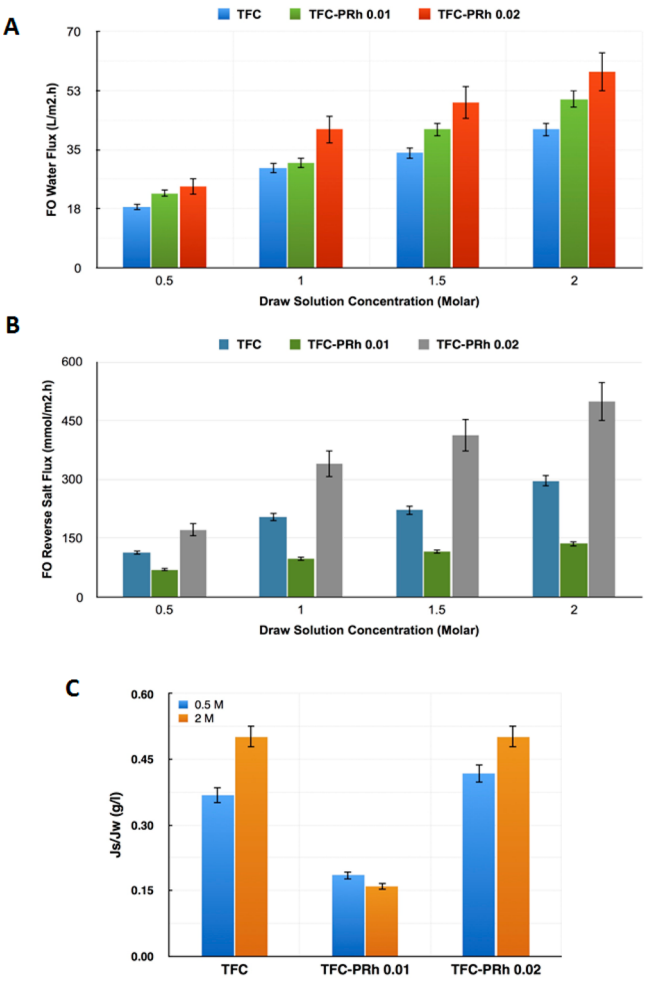

Figure 6. Performance evaluation of the TFC and TFC-PRh membranes as a function of the DS concentration: (A) FO water flux, (B) FO reverse solute flux, and (C) J_s/J_w ratio.

indicate that the FO performance of the membranes was improved by incorporating PRh-NPs into the polyamide active layer. The PRh nanoparticle incorporation creates a looser structure, a more hydrophilic surface, and a thinner active layer compared to that of a pristine TFC membrane (Figure 6a). As the driving force increased through increasing the NaCl concentration in DS, J_w of the membranes was also increased. In addition, J_s increased with the DS concentration due to a higher salt concentration gradient at the membrane surface (Figure 6b). Moreover, from Figure 6b, it can be seen that J_s of the TFC-PRh-0.01 membrane is considerably lower than those of the TFC and TFC-PRh-0.02 membranes. A loose polyamide structure may be formed at higher loading levels of PRh-NPs (e.g., 0.02 wt %), which decreases J_s. In a FO process, an important parameter indicating membrane performance is the specific solute flux (J_s/J_w). The J_s/J_w value of the TFC and TFC-PRh membranes are given in Figure 6c. A lower J_s/J_w value is preferred and indicates a higher selectivity and a higher water transport for a FO membrane.[70] A significant decrease in J_s/J_w was observed for the TFC-PRh-0.01 membrane, pointing to significant improvement in both water transport and selectivity with this level of PRh loading.

Bactericidal Activity of the TFC and TFC-PRh Membranes. The number of attached viable cells decreased significantly on the surface of the TFC-PRh-0.01 membrane compared to the pristine TFC membrane (Figure 7a and 7b), which implies that loading the PRh-NPs into the polyamide active layer imparted a strong antimicrobial property to the surface of the TFC-PRh membranes. The bacterial inactivation of over 89% and 92% was achieved for the TFC-PRh-0.01 membrane when exposed to *E. coli* and *S. aureus* bacteria, respectively.

To investigate the bactericidal activity of the TFC-PRh-0.01 membrane further, the fluorescence microscopy images of the TFC and TFC-PRh-0.01 membranes were taken after contacting with *E. coli* bacterial suspension (Figure 7d). The fluorescence images after live (green)/dead (red) staining indicated that the number of live bacteria on the surface of the TFC-PRh-0.01 membrane were much less than that of the TFC membranes. The live/dead cell ratio on the surface of the TFC membrane is about 86%, while this ratio is about 24% for the TFC-PRh-0.01 membrane, implying improved bactericidal properties of the TFC-PRh-0.01 membrane. It should be noted that this bactericidal activity was achieved with a very low concentration of the PRh-NPs (0.01 wt %). The superior bactericidal property of the TFC-PRh-0.01 membranes can be attributed to the low aggregation and the uniform distribution of PRh-NPs over/into the polyamide active layer of the membranes, as can be seen in the high magnification SEM images (Figure 3). Because of the unshared electron pairs in their sulfur and oxygen groups, the PRh-NPs provide the TFC-PRh membranes with the bactericidal property.[72] Moreover, the tertiary amide groups in the PRh structure can be partially protonated in aqueous solutions, creating positive charges.[75] These positively charged parts can interact with the structure of the bacteria lipid bilayer, causing cytoplasm outflow and the bacteria death.[47]

Antifouling and Antibiofouling Assessment of the Membranes. The normalized water flux of the TFC and TFC-PRh membranes during filtration of solutions containing sodium alginate and *E. coli* bacteria are shown in Figure 8. During filtration of both sodium alginate and *E. coli* solutions, a gradual water flux decline was observed for all membranes indicating

DOI: 10.1021/acs.est.8b00804
Environ. Sci. Technol. 2018, 52, 5246−5258

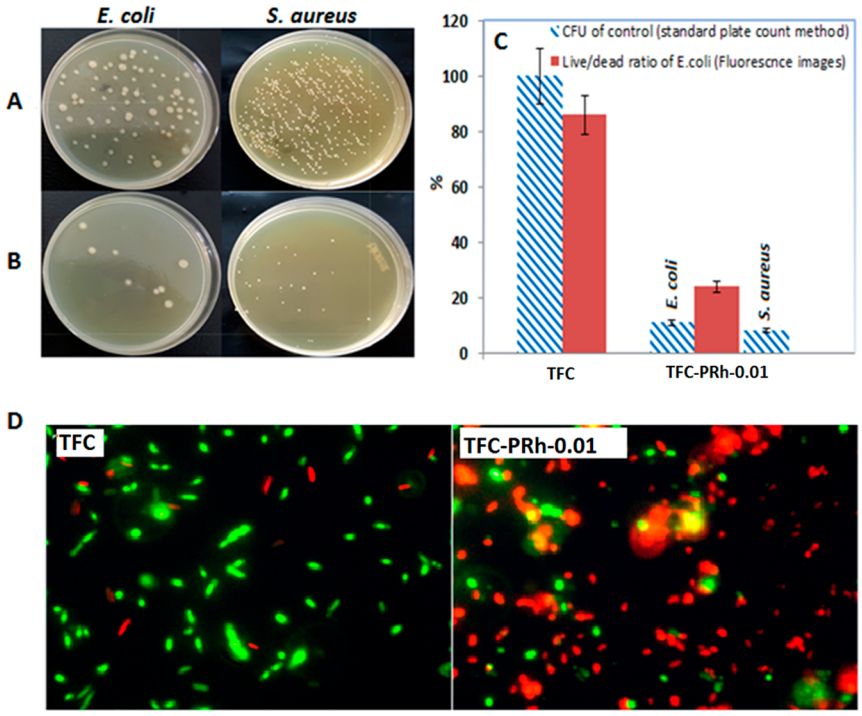

Figure 7. (A, B) Antimicrobial properties of the TFC (top) and TFC-PRh-0.01 (bottom) membranes after exposing to *E. coli* and *S. aureus* bacterial cells for 1 h. (C) Percentage of colony forming units (CFU) of *E. coli* and *S. aureus* cells relative to that on the pristine TFC membrane (control membrane) and quantitative analysis of live (green)/dead (red) *E. coli* ratios (percent) on the TFC and TFC-PRh-0.01 membranes calculated from fluorescence images. (D) Fluorescence microscopy images of *E. coli* on the TFC and TFC-PRh-0.01 membranes.

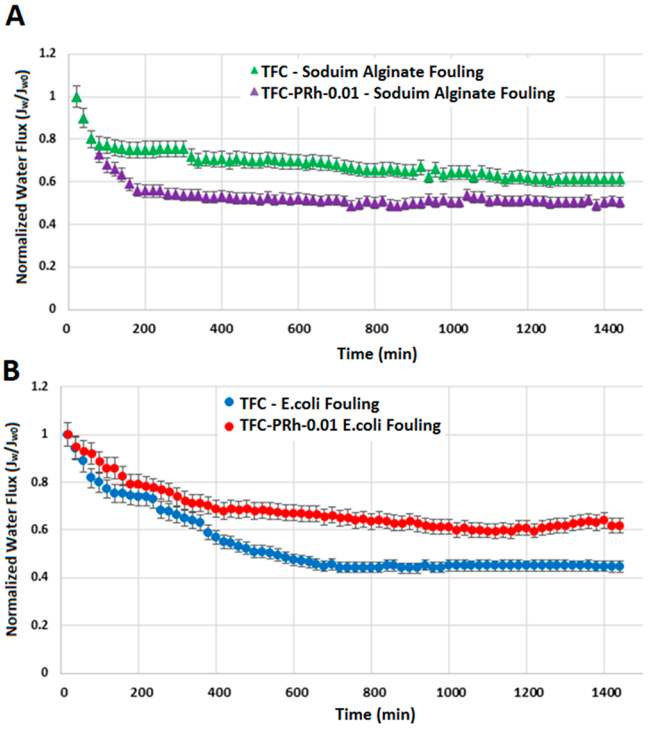

Figure 8. Normalized water fluxes of the TFC and TFC-PRh-0.01 membranes vs time during FO dynamic fouling tests. (A) Normalized water fluxes of the membranes in organic fouling experiments using sodium alginate, and (B) normalized water fluxes of the membranes in biofouling experiments using *E. coli*.

polysaccharide and bacteria adhesion and hence fouling on the membrane surface. In case of organic fouling experiments (Figure 8a), the development of polysaccharide layer on the surface of the pristine TFC membrane resulted in a water flux decline of about 50% while the TFC-PRh-0.01 membranes showed a flux decline of around 38%. Furthermore, the nitrogen atoms of PRh-NPs can attract water molecules as hydrogen acceptors and form a hydration layer to hinder the SA accumulation.[76] Alternatively, the reaction between the residual hydrolyzed acyl chloride groups and PRh-NPs can result in less carboxylic-groups active sites,[76] leading to improved resistance to SA fouling.

During filtration of the solution containing *E. coli,* the FO water flux of the TFC membrane dropped about 55% (Figure 8b). On the other hand, the TFC-PRh-0.01 membrane showed only a 37% flux decline. These results point to the better resistance of the TFC-PRh-0.01 membrane against organic and biofouling compared to the TFC membrane. The more enhanced hydrophilicity and more smooth surfaces of the TFC-PRh-0.01 membrane contribute to the improved organic and biofouling resistance of the membranes. In addition, the remarkable antimicrobial property of the TFC-PRh-0.01 membrane surface combined with the reduced bacteria adhesion prevented biofilm formation, leading to the improved anti-biofouling of the TFC-PRh-0.01 membrane.

■ ASSOCIATED CONTENT

Supporting Information

The Supporting Information is available free of charge on the ACS Publications website at DOI: 10.1021/acs.est.8b00804.

Characterization of TFC and TFC-PRh membranes, molecular dynamic simulations, antimicrobial activity assessment of the membranes, FO membrane fouling and biofouling assessment pathway, and characterization of PRh nanoparticles (PDF)

DOI: 10.1021/acs.est.8b00804
Environ. Sci. Technol. 2018, 52, 5246−5258

AUTHOR INFORMATION

Corresponding Authors

*E-mail: ahmadrahimpour@nit.ac.ir. Tel./fax: 98-11-32334204.
*E-mail: soroushm@drexel.edu. Tel.: 1-215-895-1710. Fax: 1-215-895-5837.

ORCID

Ahmad Arabi Shamsabadi: 0000-0002-9726-2466

Notes

The authors declare no competing financial interest.

REFERENCES

(1) Emadzadeh, D.; Lau, W.; Matsuura, T.; Hilal, N.; Ismail, A. The potential of thin film nanocomposite membrane in reducing organic fouling in forward osmosis process. *Desalination* **2014**, *348*, 82−88.

(2) Pinnau, I.; Freeman, B. D. *Membrane Formation and Modification*; American Chemical Society: Washington, DC, 2000.

(3) Wang, K. Y.; Chung, T. S.; Amy, G. Developing thin-film-composite forward osmosis membranes on the PES/SPSf substrate through interfacial polymerization. *AIChE J.* **2012**, *58* (3), 770−781.

(4) Wang, X.; Wang, X.; Xiao, P.; Li, J.; Tian, E.; Zhao, Y.; Ren, Y. High water permeable free-standing cellulose triacetate/graphene oxide membrane with enhanced antibiofouling and mechanical properties for forward osmosis. *Colloids Surf., A* **2016**, *508*, 327−335.

(5) Perreault, F.; Tousley, M. E.; Elimelech, M. Thin-film composite polyamide membranes functionalized with biocidal graphene oxide nanosheets. *Environ. Sci. Technol. Lett.* **2014**, *1* (1), 71−76.

(6) Amini, M.; Jahanshahi, M.; Rahimpour, A. Synthesis of novel thin film nanocomposite (TFN) forward osmosis membranes using functionalized multi-walled carbon nanotubes. *J. Membr. Sci.* **2013**, *435*, 233−241.

(7) Tiraferri, A.; Kang, Y.; Giannelis, E. P.; Elimelech, M. Super-hydrophilic thin-film composite forward osmosis membranes for organic fouling control: fouling behavior and antifouling mechanisms. *Environ. Sci. Technol.* **2012**, *46* (20), 11135−11144.

(8) Hu, M.; Zheng, S.; Mi, B. Organic fouling of graphene oxide membranes and its implications for membrane fouling control in engineered osmosis. *Environ. Sci. Technol.* **2016**, *50* (2), 685−693.

(9) Romero-Vargas Castrillón, S.; Lu, X.; Shaffer, D. L.; Elimelech, M. Amine enrichment and poly (ethylene glycol)(PEG) surface modification of thin-film composite forward osmosis membranes for organic fouling control. *J. Membr. Sci.* **2014**, *450*, 331−339.

(10) Pan, Y.; Ma, L.; Lin, S.; Zhang, Y.; Cheng, B.; Meng, J. One-step bimodel grafting via a multicomponent reaction toward antifouling and antibacterial TFC RO membranes. *J. Mater. Chem. A* **2016**, *4* (41), 15945−15960.

(11) Yu, H.-Y.; Kang, Y.; Liu, Y.; Mi, B. Grafting polyzwitterions onto polyamide by click chemistry and nucleophilic substitution on nitrogen: A novel approach to enhance membrane fouling resistance. *J. Membr. Sci.* **2014**, *449*, 50−57.

(12) Li, J.; Yin, L.; Qiu, G.; Li, X.; Liu, Q.; Xie, J. A photo-bactericidal thin film composite membrane for forward osmosis. *J. Mater. Chem. A* **2015**, *3* (13), 6781−6786.

(13) Liu, C.; Faria, A. F.; Ma, J.; Elimelech, M. Mitigation of Biofilm Development on Thin-Film Composite Membranes Functionalized with Zwitterionic Polymers and Silver Nanoparticles. *Environ. Sci. Technol.* **2017**, *51* (1), 182−191.

(14) Liu, Q.; Qiu, G.; Zhou, Z.; Li, J.; Amy, G. L.; Xie, J.; Lee, J. Y. An Effective Design of Electrically Conducting Thin-Film Composite (TFC) Membranes for Bio and Organic Fouling Control in Forward Osmosis (FO). *Environ. Sci. Technol.* **2016**, *50* (19), 10596−10605.

(15) Ben-Sasson, M.; Lu, X.; Bar-Zeev, E.; Zodrow, K. R.; Nejati, S.; Qi, G.; Giannelis, E. P.; Elimelech, M. In situ formation of silver nanoparticles on thin-film composite reverse osmosis membranes for biofouling mitigation. *Water Res.* **2014**, *62*, 260−270.

(16) Zhang, M.; Zhang, K.; De Gusseme, B.; Verstraete, W.; Field, R. The antibacterial and anti-biofouling performance of biogenic silver nanoparticles by Lactobacillus fermentum. *Biofouling* **2014**, *30* (3), 347−357.

(17) Park, S.-H.; Ko, Y.-S.; Park, S.-J.; Lee, J. S.; Cho, J.; Baek, K.-Y.; Kim, I. T.; Woo, K.; Lee, J.-H. Immobilization of silver nanoparticle-decorated silica particles on polyamide thin film composite membranes for antibacterial properties. *J. Membr. Sci.* **2016**, *499*, 80−91.

(18) Diagne, F.; Malaisamy, R.; Boddie, V.; Holbrook, R. D.; Eribo, B.; Jones, K. L. Polyelectrolyte and silver nanoparticle modification of microfiltration membranes to mitigate organic and bacterial fouling. *Environ. Sci. Technol.* **2012**, *46* (7), 4025−4033.

(19) Ben-Sasson, M.; Zodrow, K. R.; Genggeng, Q.; Kang, Y.; Giannelis, E. P.; Elimelech, M. Surface functionalization of thin-film composite membranes with copper nanoparticles for antimicrobial surface properties. *Environ. Sci. Technol.* **2014**, *48* (1), 384−393.

(20) Li, Q.; Chen, S. L.; Jiang, W. C. Durability of nano ZnO antibacterial cotton fabric to sweat. *J. Appl. Polym. Sci.* **2007**, *103* (1), 412−416.

(21) Kim, E.-S.; Hwang, G.; Gamal El-Din, M.; Liu, Y. Development of nanosilver and multi-walled carbon nanotubes thin-film nanocomposite membrane for enhanced water treatment. *J. Membr. Sci.* **2012**, *394-395*, 37−48.

(22) Leong, S.; Razmjou, A.; Wang, K.; Hapgood, K.; Zhang, X.; Wang, H. TiO 2 based photocatalytic membranes: a review. *J. Membr. Sci.* **2014**, *472*, 167−184.

(23) Zirehpour, A.; Rahimpour, A.; Ulbricht, M. Nano-sized metal organic framework to improve the structural properties and desalination performance of thin film composite forward osmosis membrane. *J. Membr. Sci.* **2017**, *531*, 59−67.

(24) Yin, J.; Yang, Y.; Hu, Z.; Deng, B. Attachment of silver nanoparticles (AgNPs) onto thin-film composite (TFC) membranes through covalent bonding to reduce membrane biofouling. *J. Membr. Sci.* **2013**, *441*, 73−82.

(25) Fu, F.; Li, L.; Liu, L.; Cai, J.; Zhang, Y.; Zhou, J.; Zhang, L. Construction of cellulose based ZnO nanocomposite films with antibacterial properties through one-step coagulation. *ACS Appl. Mater. Interfaces* **2015**, *7* (4), 2597−2606.

(26) Mauter, M. S.; Wang, Y.; Okemgbo, K. C.; Osuji, C. O.; Giannelis, E. P.; Elimelech, M. Antifouling ultrafiltration membranes via post-fabrication grafting of biocidal nanomaterials. *ACS Appl. Mater. Interfaces* **2011**, *3* (8), 2861−2868.

(27) Daer, S.; Kharraz, J.; Giwa, A.; Hasan, S. W. Recent applications of nanomaterials in water desalination: a critical review and future opportunities. *Desalination* **2015**, *367*, 37−48.

(28) Ong, C.; Goh, P.; Lau, W.; Misdan, N.; Ismail, A. Nanomaterials for biofouling and scaling mitigation of thin film composite membrane: a review. *Desalination* **2016**, *393*, 2−15.

(29) Foye, W. O.; Tovivich, P. N-glucopyranosyl-5-aralkylidenerhodanines: Synthesis and antibacterial and antiviral activities. *J. Pharm. Sci.* **1977**, *66* (11), 1607−1611.

(30) Sudo, K.; Matsumoto, Y.; Matsushima, M.; Fujiwara, M.; Konno, K.; Shimotohno, K.; Shigeta, S.; Yokota, T. Novel hepatitis C virus protease inhibitors: thiazolidine derivatives. *Biochem. Biophys. Res. Commun.* **1997**, *238* (2), 643−647.

(31) Habib, N.; Rida, S.; Badawey, E.; Fahmy, H.; Ghozlan, H. Synthesis and antimicrobial activity of rhodanine derivatives. *Eur. J. Med. Chem.* **1997**, *32* (9), 759−762.

(32) Bonde, C. G.; Gaikwad, N. J. Synthesis and preliminary evaluation of some pyrazine containing thiazolines and thiazolidinones as antimicrobial agents. *Bioorg. Med. Chem.* **2004**, *12* (9), 2151−2161.

(33) Kong, H.; Song, J.; Jang, J. One-step fabrication of magnetic γ-Fe 2 O 3/polyrhodanine nanoparticles using in situ chemical oxidation polymerization and their antibacterial properties. *Chem. Commun.* **2010**, *46* (36), 6735−6737.

(34) Schatz, G. C. Using theory and computation to model nanoscale properties. *Proc. Natl. Acad. Sci. U. S. A.* **2007**, *104* (17), 6885−6892.

(35) Hughes, Z. E.; Gale, J. D. Molecular dynamics simulations of the interactions of potential foulant molecules and a reverse osmosis membrane. *J. Mater. Chem.* **2012**, *22* (1), 175−184.

DOI: 10.1021/acs.est.8b00804
Environ. Sci. Technol. 2018, 52, 5246−5258

(36) Choi, W.; Choi, J.; Bang, J.; Lee, J.-H. Layer-by-layer assembly of graphene oxide nanosheets on polyamide membranes for durable reverse-osmosis applications. *ACS Appl. Mater. Interfaces* **2013**, *5* (23), 12510−12519.
(37) Chen, Y.-R.; Chen, L.-H.; Chang, K.-S.; Chen, T.-H.; Lin, Y.-F.; Tung, K.-L. Structural characteristics and transport behavior of triptycene-based PIMs membranes: A combination study using ab initio calculation and molecular simulations. *J. Membr. Sci.* **2016**, *514*, 114−124.
(38) Tiraferri, A.; Yip, N. Y.; Straub, A. P.; Romero-Vargas Castrillon, S.; Elimelech, M. A method for the simultaneous determination of transport and structural parameters of forward osmosis membranes. *J. Membr. Sci.* **2013**, *444*, 523−538.
(39) Perreault, F.; Jaramillo, H.; Xie, M.; Ude, M.; Nghiem, L. D.; Elimelech, M. Biofouling mitigation in forward osmosis using graphene oxide functionalized thin-film composite membranes. *Environ. Sci. Technol.* **2016**, *50* (11), 5840−5848.
(40) Zirehpour, A.; Rahimpour, A.; Arabi Shamsabadi, A.; Sharifian Gh, M.; Soroush, M. Mitigation of Thin-Film Composite Membrane Biofouling via Immobilizing Nano-Sized Biocidal Reservoirs in the Membrane Active Layer. *Environ. Sci. Technol.* **2017**, *51* (10), 5511−5522.
(41) Ghanbari, M.; Emadzadeh, D.; Lau, W.; Matsuura, T.; Ismail, A. Synthesis and characterization of novel thin film nanocomposite reverse osmosis membranes with improved organic fouling properties for water desalination. *RSC Adv.* **2015**, *5* (27), 21268−21276.
(42) Tang, C.; Li, X.; Li, Z.; Hao, J. Interfacial Hydrogen Bonds and Their Influence Mechanism on Increasing the Thermal Stability of Nano-SiO2-Modified Meta-Aramid Fibres. *Polymers* **2017**, *9* (10), 504.
(43) Jeffrey, G. A.; Jeffrey, G. A. *An Introduction to Hydrogen Bonding*; Oxford University Press: New York, 1997; Vol. *32*.
(44) Rahimpour, A.; Jahanshahi, M.; Mollahosseini, A.; Rajaeian, B. Structural and performance properties of UV-assisted TiO 2 deposited nano-composite PVDF/SPES membranes. *Desalination* **2012**, *285*, 31−38.
(45) Ghorbani, M.; Alizadeh, B.; Salehi, M. A. Study on novel poly (vinyl pyrrolidone) doped MWCNTs/polyrhodanine nanocomposites: Synthesis, characterization, and thermal performance. *Fullerenes, Nanotubes, Carbon Nanostruct.* **2016**, *24* (9), 604−609.
(46) Silverstein, R. M.; Webster, F. X.; Kiemle, D. J.; Bryce, D. L. *Spectrometric Identification of Organic Compounds*; John Wiley & Sons, 2014.
(47) Kardaş, G.; Solmaz, R. Electrochemical synthesis and characterization of a new conducting polymer: Polyrhodanine. *Appl. Surf. Sci.* **2007**, *253* (7), 3402−3407.
(48) Ozkan, S.; Unal, H. I.; Yılmaz, E.; Suludere, Z. Electrokinetic and antibacterial properties of needle like-TiO_2/polyrhodanine core/shell hybrid nanostructures. *J. Appl. Polym. Sci.* **2015**, *132* (9), 41554.
(49) Emadzadeh, D.; Lau, W.; Rahbari-Sisakht, M.; Ilbeygi, H.; Rana, D.; Matsuura, T.; Ismail, A. Synthesis, modification and optimization of titanate nanotubes-polyamide thin film nanocomposite (TFN) membrane for forward osmosis (FO) application. *Chem. Eng. J.* **2015**, *281*, 243−251.
(50) Xia, S.; Yao, L.; Zhao, Y.; Li, N.; Zheng, Y. Preparation of graphene oxide modified polyamide thin film composite membranes with improved hydrophilicity for natural organic matter removal. *Chem. Eng. J.* **2015**, *280*, 720−727.
(51) Kim, H. J.; Lim, M.-Y.; Jung, K. H.; Kim, D.-G.; Lee, J.-C. High-performance reverse osmosis nanocomposite membranes containing the mixture of carbon nanotubes and graphene oxides. *J. Mater. Chem. A* **2015**, *3* (13), 6798−6809.
(52) Vatanpour, V.; Madaeni, S. S.; Rajabi, L.; Zinadini, S.; Derakhshan, A. A. Boehmite nanoparticles as a new nanofiller for preparation of antifouling mixed matrix membranes. *J. Membr. Sci.* **2012**, *401-402*, 132−143.
(53) Hu, D.; Xu, Z.-L.; Chen, C. Polypiperazine-amide nanofiltration membrane containing silica nanoparticles prepared by interfacial polymerization. *Desalination* **2012**, *301*, 75−81.
(54) Chen, X.; Zhang, W.; Lin, Y.; Cai, Y.; Qiu, M.; Fan, Y. Preparation of high-flux γ-alumina nanofiltration membranes by using a modified sol−gel method. *Microporous Mesoporous Mater.* **2015**, *214*, 195−203.
(55) Baroña, G. N. B.; Lim, J.; Choi, M.; Jung, B. Interfacial polymerization of polyamide-aluminosilicate SWNT nanocomposite membranes for reverse osmosis. *Desalination* **2013**, *325*, 138−147.
(56) Lind, M. L.; Ghosh, A. K.; Jawor, A.; Huang, X.; Hou, W.; Yang, Y.; Hoek, E. M. Influence of zeolite crystal size on zeolite-polyamide thin film nanocomposite membranes. *Langmuir* **2009**, *25* (17), 10139−10145.
(57) Tang, C. Y.; She, Q.; Lay, W. C.; Wang, R.; Fane, A. G. Coupled effects of internal concentration polarization and fouling on flux behavior of forward osmosis membranes during humic acid filtration. *J. Membr. Sci.* **2010**, *354* (1), 123−133.
(58) Kim, E.-S.; Deng, B. Fabrication of polyamide thin-film nanocomposite (PA-TFN) membrane with hydrophilized ordered mesoporous carbon (H-OMC) for water purifications. *J. Membr. Sci.* **2011**, *375* (1), 46−54.
(59) Yin, J.; Kim, E.-S.; Yang, J.; Deng, B. Fabrication of a novel thin-film nanocomposite (TFN) membrane containing MCM-41 silica nanoparticles (NPs) for water purification. *J. Membr. Sci.* **2012**, *423-424*, 238−246.
(60) Huang, H.; Qu, X.; Ji, X.; Gao, X.; Zhang, L.; Chen, H.; Hou, L. Acid and multivalent ion resistance of thin film nanocomposite RO membranes loaded with silicalite-1 nanozeolites. *J. Mater. Chem. A* **2013**, *1* (37), 11343−11349.
(61) Khorshidi, B.; Thundat, T.; Fleck, B.; Sadrzadeh, M. Thin film composite polyamide membranes: parametric study on the influence of synthesis conditions. *RSC Adv.* **2015**, *5* (68), 54985−54997.
(62) Benavente, J.; Vázquez, M. Effect of age and chemical treatments on characteristic parameters for active and porous sublayers of polymeric composite membranes. *J. Colloid Interface Sci.* **2004**, *273* (2), 547−555.
(63) Xu, L.; Xu, J.; Shan, B.; Wang, X.; Gao, C. Novel thin-film composite membranes via manipulating the synergistic interaction of dopamine and m-phenylenediamine for highly efficient forward osmosis desalination. *J. Mater. Chem. A* **2017**, *5* (17), 7920−7932.
(64) Boussu, K.; De Baerdemaeker, J.; Dauwe, C.; Weber, M.; Lynn, K. G.; Depla, D.; Aldea, S.; Vankelecom, I. F.; Vandecasteele, C.; Van der Bruggen, B. Physico-chemical characterization of nanofiltration membranes. *ChemPhysChem* **2007**, *8* (3), 370−379.
(65) Tang, C. Y.; Kwon, Y.-N.; Leckie, J. O. Probing the nano-and micro-scales of reverse osmosis membranes—a comprehensive characterization of physiochemical properties of uncoated and coated membranes by XPS, TEM, ATR-FTIR, and streaming potential measurements. *J. Membr. Sci.* **2007**, *287* (1), 146−156.
(66) Tang, C. Y.; Kwon, Y.-N.; Leckie, J. O. Effect of membrane chemistry and coating layer on physiochemical properties of thin film composite polyamide RO and NF membranes: II. Membrane physiochemical properties and their dependence on polyamide and coating layers. *Desalination* **2009**, *242* (1−3), 168−182.
(67) Briggs, D.; Beamson, G. XPS studies of the oxygen 1s and 2s levels in a wide range of functional polymers. *Anal. Chem.* **1993**, *65* (11), 1517−1523.
(68) López, G. P.; Castner, D. G.; Ratner, B. D. XPS O 1s binding energies for polymers containing hydroxyl, ether, ketone and ester groups. *Surf. Interface Anal.* **1991**, *17* (5), 267−272.
(69) Feng, X.; Song, M.-K.; Stolte, W. C.; Gardenghi, D.; Zhang, D.; Sun, X.; Zhu, J.; Cairns, E. J.; Guo, J. Understanding the degradation mechanism of rechargeable lithium/sulfur cells: a comprehensive study of the sulfur−graphene oxide cathode after discharge−charge cycling. *Phys. Chem. Chem. Phys.* **2014**, *16* (32), 16931−16940.
(70) Phillip, W. A.; Yong, J. S.; Elimelech, M. Reverse draw solute permeation in forward osmosis: modeling and experiments. *Environ. Sci. Technol.* **2010**, *44* (13), 5170−5176.
(71) Moaddeb, M.; Koros, W. J. Gas transport properties of thin polymeric membranes in the presence of silicon dioxide particles. *J. Membr. Sci.* **1997**, *125* (1), 143−163.

DOI: 10.1021/acs.est.8b00804
Environ. Sci. Technol. 2018, 52, 5246−5258

(72) Seyfriedsberger, G.; Rametsteiner, K.; Kern, W. Polyethylene compounds with antimicrobial surface properties. *Eur. Polym. J.* **2006**, *42* (12), 3383−3389.
(73) Song, X.; Zhou, Q.; Zhang, T.; Xu, H.; Wang, Z. Pressure-assisted preparation of graphene oxide quantum dot-incorporated reverse osmosis membranes: antifouling and chlorine resistance potentials. *J. Mater. Chem. A* **2016**, *4* (43), 16896−16905.
(74) Wu, H.; Tang, B.; Wu, P. Optimizing polyamide thin film composite membrane covalently bonded with modified mesoporous silica nanoparticles. *J. Membr. Sci.* **2013**, *428*, 341−348.
(75) Gelman, M. A.; Weisblum, B.; Lynn, D. M.; Gellman, S. H. Biocidal activity of polystyrenes that are cationic by virtue of protonation. *Org. Lett.* **2004**, *6* (4), 557−560.
(76) Shen, L.; Zhang, X.; Zuo, J.; Wang, Y. Performance enhancement of TFC FO membranes with polyethyleneimine modification and post-treatment. *J. Membr. Sci.* **2017**, *534*, 46−58.

DOI: 10.1021/acs.est.8b00804
Environ. Sci. Technol. 2018, 52, 5246−5258